CHEMISTRY OF MATERIALS

Article

pubs.acs.org/cm

Controlled Synthesis of Atomically Thin 1T-TaS_2 for Tunable Charge Density Wave Phase Transitions

Wei Fu,[†] Yu Chen,[‡] Junhao Lin,[*,§] Xuewen Wang,[†] Qingsheng Zeng,[†] Jiadong Zhou,[†] Lu Zheng,[†] Hong Wang,[†] Yongmin He,[†] Haiyong He,[†] Qundong Fu,[†] Kazutomo Suenaga,[§] Ting Yu,[*,‡] and Zheng Liu[*,†,∥]

[†]Centre for Programmed Materials, School of Materials Science and Engineering, Nanyang Technological University, 50 Nanyang Avenue, 639798, Singapore

[‡]School of Physical and Mathematical Sciences, Nanyang Technological University, 21 Nanyang Link, 637371, Singapore

[§]National Institute of Advanced Industrial Science and Technology (AIST), Tsukuba 305-8565, Japan

[∥]NOVITAS, Nanoelectronics Centre of Excellence, School of Electrical and Electronic Engineering, Nanyang Technological University, 639798, Singapore

Supporting Information

ABSTRACT: The charge density wave (CDW) in two-dimensional (2D) materials is attracting substantial interest because of its magnificent many-body collective phenomena. Various CDW phases have been observed in several 2D materials before they reach the phase of superconductivity. However, to date, the atomically thin CDW materials were mainly fabricated by mechanically exfoliating from their bulk counterparts, which leads to low production yield and small sample sizes. Here, we report the controlled synthesis of atomically thin 1T-TaS_2, a typical CDW material, by a chemical vapor deposition (CVD) method. The high quality of as-grown 1T-TaS_2 has been confirmed by complementary characterization technologies. Moreover, the thickness-dependent CDW phase transitions have been revealed in these ultrathin flakes by temperature-dependent Raman spectra. This work opens up a new window for the large-scale synthesis of ultrathin CDW materials and sheds light on the fabrication of next-generation electronic devices.

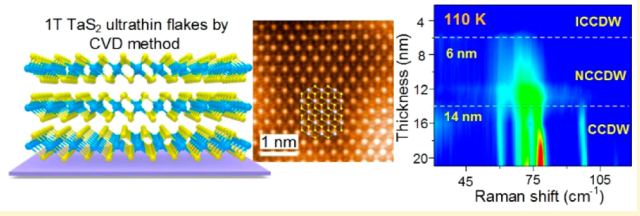

Charge density wave (CDW) materials have attracted a lot attention over the past few years,[1,2] and the manipulation of many-body states in these CDW materials becomes a promising approach for designing next-generation electronic devices.[3,4] It is believed that the dimensionality of the CDW materials greatly affects instability of CDW states.[5] With reduction of the dimensionality, Peierls instabilities and electron−phonon interactions are strongly enhanced, which triggers a stronger CDW effect.[6] Thus, two-dimensional (2D) materials, which can be isolated into atomically thin layers, show great potential for CDW applications. For example, the highly unusual enhancement of CDWs was observed in atomically thin $NbSe_2$ due to the significantly enhanced electron−phonon interactions,[5] and the room-temperature CDWs phase transitions are realized in thin flakes of 1T-TaS_2 and $TiSe_2$ through the method of gate-controlled Li^+ intercalation.[7−9] However, to our best knowledge, the fabrication of ultrathin 2D layers mainly relies on the mechanical exfoliation method, which suffers from the low production yield and small sample sizes.[10−12]

The chemical vapor deposition (CVD) method, involving the chemical reactions of gaseous reactants on a heated substrate surface, is regarded as one of the main processing methods for synthesis of 2D materials.[13,14] It can produce large-size and high-quality 2D materials, such as graphene, MoS_2,[15−17] WS_2,[18] and BN,[19,20] with controlled thickness. Therefore, the CVD method could be employed as a swift and effective way to synthesize high-quality 2D CDW materials in a controlled manner. In this work, we have demonstrated the controlled synthesis of atomically thin 1T-TaS_2,[21−23] via the CVD method. The thicknesses of 1T-TaS_2 can be tuned from two to several hundred nanometers, as revealed by atomic force microscopy (AFM). Their high quality has been confirmed by scanning transmission electron microscope (STEM) and electron energy loss spectra (EELS). With the help of *in situ* temperature-dependent Raman spectroscopy, we also revealed the thickness-dependent CDW phase transitions in our CVD-grown samples. Briefly, three phases can be found in our CVD-grown 1T-TaS_2: incommensurate CDW (ICCDW), nearly commensurate CDW (NCCDW), and commensurate CDW (CCDW). For a sample of a thickness above 14 nm, a CCDW phase was observed. As its thickness reaches 14 nm, the transition from CCDW to NCCDW phase was identified. As the thickness reaches 6 nm, the transition from the CCDW to

Received: June 10, 2016
Revised: October 17, 2016
Published: October 18, 2016

ACS Publications © XXXX American Chemical Society

DOI: 10.1021/acs.chemmater.6b02334
Chem. Mater. XXXX, XXX, XXX−XXX

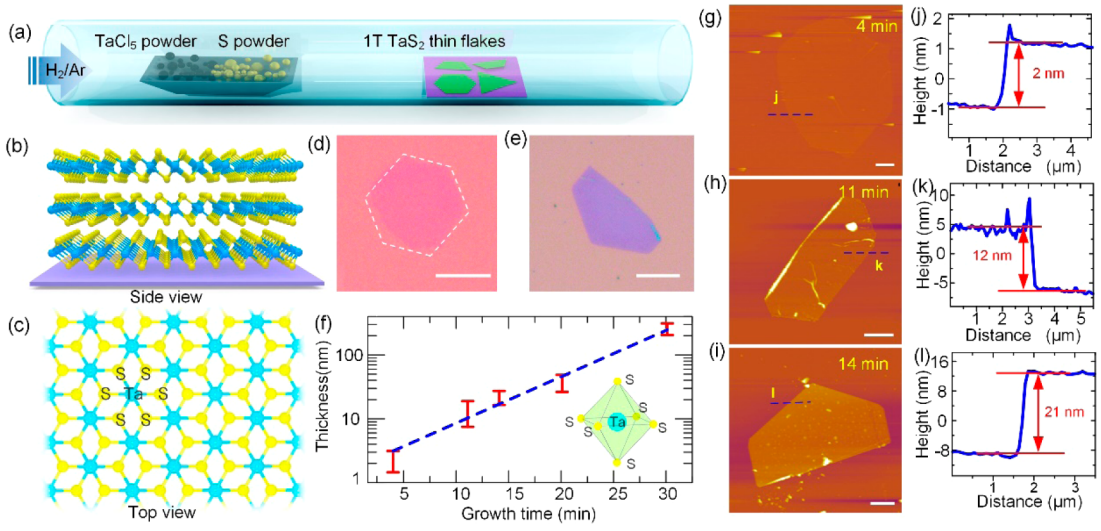

Figure 1. Controlled synthesis of ultrathin 1T-TaS_2 crystals via a CVD method. (a) Schematic of CVD setup for the growth of 1T-TaS_2 on a SiO_2/Si substrate with tantalum pentachloride powder and sulfur powder used as the precursors. (b, c) Crystal structure of distorted 1T-TaS_2 on a SiO_2/Si substrate. (d, e) Optical images of 1T-TaS_2 ultrathin flakes. (f) The controlled thicknesses of 1T-TaS_2 at different growth times. The inset shows an octahedral arrangement of the central Ta atom coordinated with S atoms. (g–l) AFM images and their corresponding height profiles of various 1T-TaS_2 at different growing times. The scale bars are 10 μm in parts d and e and 2 μm in parts g, h, and i.

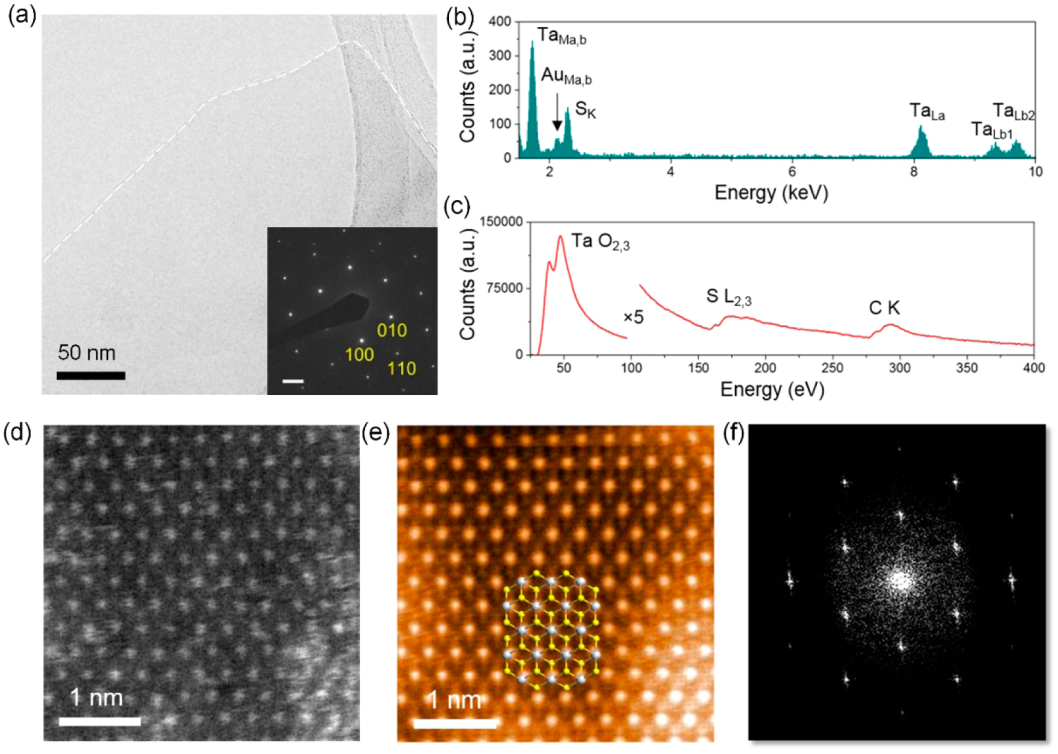

Figure 2. TEM/STEM characterization of a 1T-TaS_2 atomically thin flake. (a) Low-resolution TEM image. Inset is the corresponding SAED patterns of the marked flake with 6-fold rotational symmetry, revealing the hexagonal structure. (b, c) EDX (b) and EELS (c) spectra of the thin flakes. Ta and S can be identified from both spectra. The occurrence of the Au signal comes from the nearby gold TEM grid bars. (d) High-resolution STEM image along the [001] direction of a monolayer region near the edge of a thin TaS_2 flake. (e) FFT filtered image of part d with enhanced visibility, showing the positions of Ta and S atoms inside the hexagonal 1T lattice, confirming the high quality of the sample. The atomic structural model is overlaid on the image. (f) FFT pattern of the region shown in part d.

NCCDW phase was observed. This controlled synthesis of large-area ultrathin CDW materials via a CVD method shows great potential for the fabrication of next-generation electronic devices.

The CVD setup for synthesizing ultrathin 1T-TaS_2 is represented in Figure 1a. The tantalum pentachloride and sulfur powder were used as the precursors of Ta and S, respectively. The SiO_2/Si wafer was chosen as preferred substrate for growth. In a typical process, the mixed powders were placed at an inlet of the tube furnace, while the SiO_2/Si wafer is located at the center of the furnace. Then, under the H_2/Ar mixture (10% H_2) carrier gas, the furnace was heated up

DOI: 10.1021/acs.chemmater.6b02334
Chem. Mater. XXXX, XXX, XXX−XXX

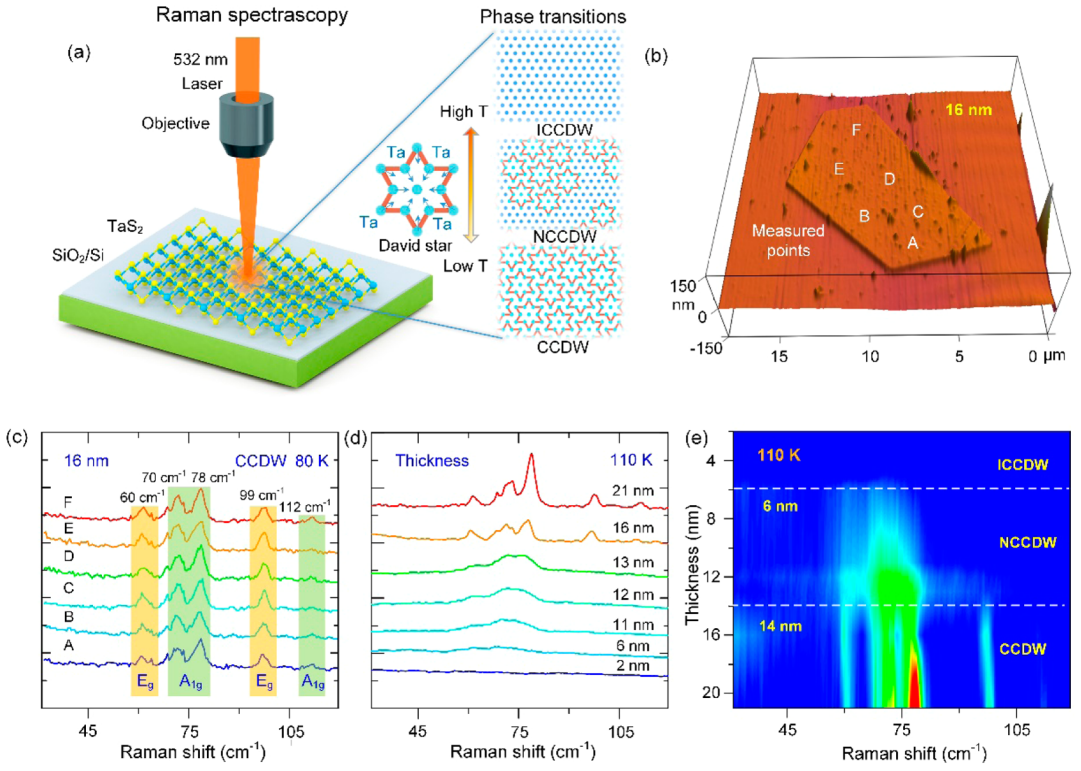

Figure 3. Raman characterization of as-grown 1T-TaS_2 samples. (a) Schematic of CDW phase transitions measured by Raman spectroscopy. (b) AFM topography of the 16-nm-thick flake, showing uniform thickness along the whole flake. Raman spectra were collected from six different points labeled in part b. (c) Raman spectra at points A–F collected at 80 K. The pronounced out-of-plane A_{1g} modes of 70, 78, and 112 cm^{-1} and in-plane E_g modes of 60 and 99 cm^{-1} indicated the existence of a CCDW state. (d, e) The thickness-dependent Raman spectra and plotted Raman map at 110 K. The presence of two broad modes of 60.5 and 71.2 cm^{-1} on 6-nm-thick sample and the splitting of 61 and 77 cm^{-1} modes into many well-resolved peaks on a 16-nm-thick sample revealed the CDW transitions of ICCDW to NCCDW and NCCDW to CCDW, respectively.

to 1093 K to chemically grow 1T-TaS_2 layers on a SiO_2/Si substrate. The side view (Figure 1b) and top view (Figure 1c) of the 1T-TaS_2 crystal structure clearly show that 1T-TaS_2 is a typically layered material. Each TaS_2 layer is composed of the hexagonally arranged Ta atoms sandwiched between two sulfur layers. Sulfur atoms coordinate the central Ta atom in an octahedral arrangement.[24,25] The weak interlayer van der Waals forces actually help in controlling the number of layers and hence the thickness of TaS_2. Figure 1d,e shows optical images of the 2-nm-thick and 11-nm-thick samples. By controlling the growing time, TaS_2 samples with different thicknesses were obtained at 1093 K, as shown in Figure 1 and Figure S1. In fact, one can estimate the thickness of TaS_2 by its contrast. Thick samples (>10 nm) are in blue while thin films like few-layered TaS_2 are in purple. In our work, the thicknesses of TaS_2 samples were accurately determined by AFM. As can be seen in Figure 1f, the thickness of TaS_2 is linearly dependent on growing time. As we changed the growing time from 4 to 30 min, the thickness of TaS_2 increased from 2 nm to above 200 nm. From the AFM images and corresponding height profiles in Figure 1g–l and Figures S2–4, we can also see that the CVD-grown TaS_2 samples are uniform for relatively large flakes (>10 μm). In addition, the X-ray diffraction patterns of a 220-nm-thick sample (in Figure S5) confirmed that the structure of our CVD-grown TaS_2 is the 1T phase (JCPDS 73-2201).[26,27]

The quality of the as-grown crystal was further examined by TEM and STEM. Figure 2a shows a TEM image of the atomically thin TaS_2 flake, displaying a uniform film with a smooth surface. The selected area electron diffraction (SAED) patterns of the 6-fold rotational symmetric diffraction patterns confirm the hexagonal structure of the CVD-grown TaS_2 at a large scale. Figure 2b,c shows the energy dispersive X-ray spectra (EDS) and EELS of the as-synthesized thin flakes, confirming its chemical composition: Ta and S elements without any other obvious impurities. Figure 2d shows a high-resolution Z-contrast STEM image of a monolayer region near the edge of the thin flakes. Ta (bright spots) and S atoms can be easily identified by their contrast. However, S atoms are nearly invisible due to the large difference of the atomic number between Ta and S. In order to reveal the position of the S atoms, a fast Fourier transformation (FFT) filtered image is provided in Figure 2e,f. Figure 2e shows clearly the displaced S_2 columns surrounding the Ta atoms, which is consistent with the 1T structural model as overlaid in the same image. These high-resolution STEM images assured the high quality of our CVD-grown TaS_2 flakes in the intrinsic 1T phase. Moreover, the X-ray photoelectron spectroscopy (XPS) was used to identify the chemical binding in the CVD-grown 1T-TaS_2 flake. The XPS results are shown in Figure S6. In the high-resolution Ta 4f spectrum, the Ta $4f_{5/2}$ and Ta $4f_{7/2}$ peaks are located at 24.7 and 22.7 eV, respectively, corresponding to Ta^{4+} from TaS_2.[28] In the high-resolution S 2p spectrum, peaks at 161 and 160 eV are from the S $2p_{1/2}$ and S $2p_{3/2}$, respectively.[29] The small amounts of Ta_2O_5 species, caused by surface oxidation of TaS_2, were also detected on the flake.

Our CVD-grown 1T-TaS_2 shows rich CDW phases. As seen in Figure 3a, 1T-TaS_2 undergoes a series of CDW transitions from metallic ICCDW, to textured NCCDW, to insulated CCDW, on lowering the temperature. The low-temperature CCDW phase is characterized by $\sqrt{13} \times \sqrt{13}$ superlattice of

DOI: 10.1021/acs.chemmater.6b02334
Chem. Mater. XXXX, XXX, XXX–XXX

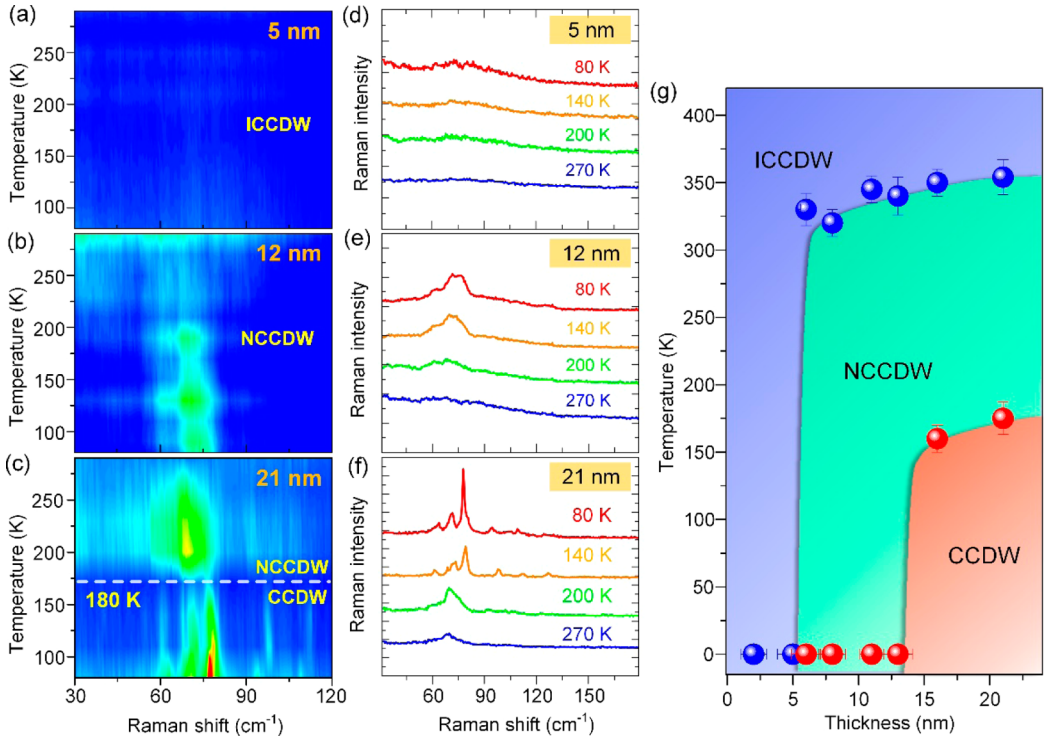

Figure 4. Thickness-dependent CDW phase transitions in CVD-grown 1T-TaS_2 thin flakes. (a–f) The Raman intensity counter maps and Raman spectra for 1T-TaS_2 flakes with different thicknesses. For a 21-nm-thick sample, as the temperature lowered to 170 K, the Raman modes around 61 and 77 cm^{-1} split into many well-resolved peaks, revealing the transition from NCCDW to CCDW. This transition was not observed in 5- and 12-nm-thick samples, because the long-range CDW coherence was destroyed by the stronger fluctuation effects. (g) The thickness-temperature phase diagram for CVD-grown samples. As the sample thickness reduced, both transitions of ICCDW/NCCDW and NCCDW/CCDW were shifted to lower temperatures, and then vanished at critical thicknesses of 6 and 14 nm, respectively.

David stars formed by 12 Ta atoms clustered around a 13th Ta atom.[30] The periodic lattice distortion creates energy gaps in the 1T-TaS_2 band structure and leaves exactly one conduction electron per David star.[31] The on-site Coulomb repulsion further localizes this conduction electron and produces a Mott insulator state.[21]

It is believed that the phonons could couple strongly to the collective modes of CDW states.[36,37] Raman spectroscopy has been a powerful tool to investigate the CDW phase transitions due to the high resolution and high sensitivity. Many additional Raman modes appear in the commensurate CDW state due to the folding of the original Brillouin zone.[32] Here, we conducted the *in situ* temperature-dependent Raman measurements on our 1T-TaS_2 samples to undertand the thickness-dependent CDW phase transitions. The 16-nm-thick sample was used in this experiment as shown in Figure 3b. First, we investigated its structural homogeneity. We selected six locations, labeled as A–F (as seen in Figure 3b), to collect the Raman spectra. The Raman spectra and plotted intensity mapping collected at 80 K are shown in Figure 3c and Figure S7, respectively. It can be seen that the pronounced out-of-plane A_{1g} modes of 70, 78, and 112 cm^{-1} and in-plane E_g modes of 60 and 99 cm^{-1} are clearly detected in the Raman spectra, indicating the existence of the CCDW state.[33,34] The homogeneous Raman mapping spectra in Figure 3c further confirms the good quality of our CVD-grown TaS_2. Figure 3d shows the Raman spectra collected at 110 K from samples with various thicknesses from 2 to 21 nm. It can be seen that, as the thickness increased, the appearance of two broad modes at 60.5 and 71.2 cm^{-1} was first observed on a 6-nm-thick sample which can be attributed to the presence of the NCCDW phase. Also, their subsequent splitting into many well-resolved peaks was detected on a 16-nm-thick sample, which corresponds to the presence of the CCDW phase. These results revealed the thickness-dependent CDW transitions.[33] It can be clearly seen from thickness-dependent Raman mapping in Figure 3e. Moreover, this result further proved the high quality of our as-grown 1T-TaS_2.

To understand the CDW phase transitions of as-grown 1T-TaS_2 samples, we conducted the *in situ* temperature-dependent Raman measurements. For a 21-nm-thick sample, Figure 4c,f shows the plotted Raman intensity map and Raman spectra at 270, 200, 140, and 80 K, respectively (complete Raman spectra are shown in Figure S8). As the temperature decreases, the Raman peaks corresponding to a NCCDW state become significantly intense. The A_g mode at 77 cm^{-1} is the strongest peak and shows a large temperature-dependent Raman shift. According to the previous reports,[32,34,35] the modes below 140 cm^{-1} are derived from the acoustic phonon branches which resulted from the vibrations of the tantalum atoms. When the temperature decreased to 170 K, the Raman modes at 61 and 77 cm^{-1} split into a few more peaks. These new modes can contribute to the increase in the number of zone center (Γ-point) phonon modes when the original Brillouin zone folds.[8] The results evidenced the phase transition from NCCDW to CCDW at 170 K, which is in agreement with various retrospective studies.[22,36,32] For a 12-nm-thick sample (complete Raman spectra shown in Figure S9), Figure 4b,e only shows the characteristic phonon modes of the NCCDW phase at frequencies of 60, 71, 77, and 97 cm^{-1} without splitting. This result dictates the suppression of a phase transition from NCCDW to CCDW at a 12-nm-thick 1T-TaS_2 flake. A similar phenomenon was also observed in ultrathin flakes at

DOI: 10.1021/acs.chemmater.6b02334
Chem. Mater. XXXX, XXX, XXX–XXX

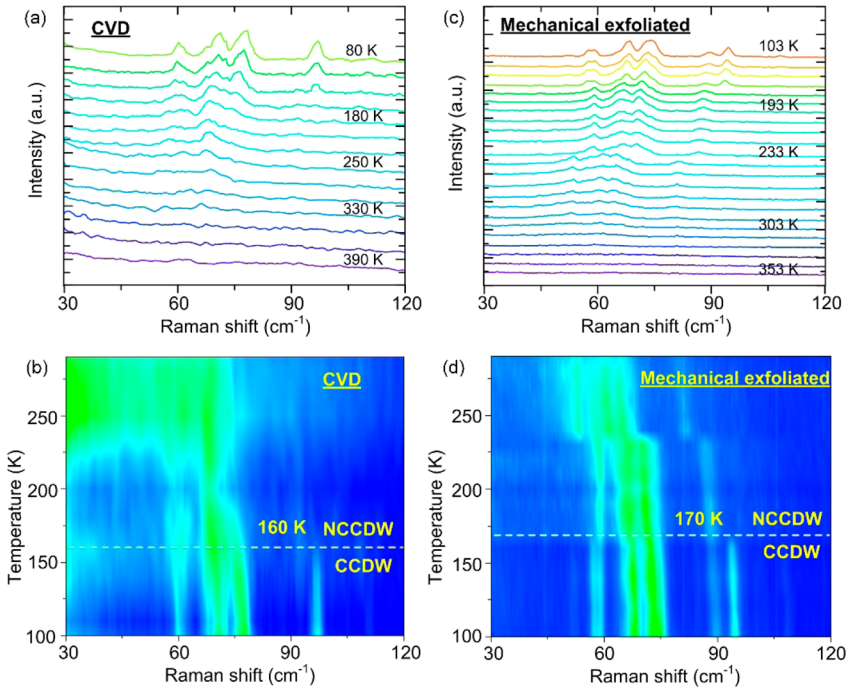

Figure 5. Phase-transition comparison between CVD-grown 1T-TaS_2 flakes and mechanically exfoliated ones. (a, b) Temperature-dependent Raman spectra and intensity maps of CVD-grown samples. (c, d) The temperature-dependent Raman spectra and intensity maps of mechanically exfoliated samples. The Raman vibration modes and transition feature from NCCDW to CCDW matches quite well for both samples, confirming the high quality of the CVD-grown samples.

thicknesses of 11 and 13 nm, which can be concluded from their Raman analysis in Figures S10 and S11. When we focused on the 5-nm-thick 1T-TaS_2 flake, no characteristic phonon modes of NCCDW were detected in Raman spectra (Figure 4a,d), revealing the suppression of a phase transition from ICCDW to NCCDW at the 5-nm-thick 1T-TaS_2 flake. Moreover, in order to clarify the thickness-dependent CDW phase transitions, we examined the thinner sample down to 2 nm. The thickness−temperature phase diagram is shown in Figure 4g. As the sample thickness was reduced, the phase transitions of ICCDW to NCCDW and NCCDW to CCDW were shifted to lower temperatures, and vanished at a critical thickness of 6 and 14 nm, respectively, demonstrating that the phase-transition temperature can be tuned by the thickness of the as-grown TaS_2.

In order to compare the property of CDW phase transitions between CVD-grown 1T-TaS_2 flakes and mechanical exfoliated samples, we also carried out *in situ* temperature-dependent Raman measurements on the mechanically exfoliated thin flake. The Raman spectra of CVD-grown and mechanically exfoliated samples are shown in Figure 5. Although both samples exhibit the similar temperature-dependent CDW phase transitions, the slight broadening of peak line width of the CVD-grown sample was observed as compared to that of the mechanically exfoliated one, which might be due to the increased lattice defects in CVD-grown samples. Moreover, the suppression of the CCDW transition from 170 to 160 K was also detected in the CVD-grown sample. The reason can be that lattice defects might have disordered the positions of Ta atoms in a superlattice of David stars, which subsequently results in the suppression of a Mott insulating state or CCDW phase.[27]

To summarize, we have developed a CVD method to synthesize metallic 1T-TaS_2 atomically thin crystals on a SiO_2/Si substrate with controlled thickness. The high quality of CVD-grown 1T-TaS_2 is confirmed by complementary characterizations like XPS, AFM, and STEM. We also identified the thickness-dependent CDW phase transitions using Raman spectroscopy. This work provides a promising way to produce high-quality 2D CDW materials and related electronics devices.

■ ASSOCIATED CONTENT

Supporting Information

The Supporting Information is available free of charge on the ACS Publications website at DOI: 10.1021/acs.chemmater.6b02334.

Methods, general characterization, Raman testing, optical images of variable-thickness flakes, AFM images and height profiles of flakes, XRD pattern, and complete Raman spectra of 1T-TaS_2 flakes with different thicknesses (PDF)

■ AUTHOR INFORMATION

Corresponding Authors

*E-mail: lin.junhao@aist.go.jp.
*E-mail: Yuting@ntu.edu.sg.
*E-mail: z.liu@ntu.edu.sg.

Author Contributions

W.F., Y.C., and J.L. contributed equally to this work.

Notes

The authors declare no competing financial interest.

■ ACKNOWLEDGMENTS

This work is supported by the Singapore National Research Foundation under NRF RF Award NRF-RF2013-08, the Ministry of Education Singapore under Grant MOE Tier 2 MOE2015-T2-2-007, MOE Tier 1 RG164/15, and the CoE Industry Research and Innovation Collaboration Programme.

DOI: 10.1021/acs.chemmater.6b02334
Chem. Mater. XXXX, XXX, XXX−XXX

T.Y. acknowledges the support from the Ministry of Education Singapore under Grant MOE Tier 1 RG100/15. J.L. and K.S. acknowledge support from the JST Research Acceleration Programme.

REFERENCES

(1) Rossnagel, K. On the origin of charge-density waves in select layered transition-metal dichalcogenides. *J. Phys.: Condens. Matter* **2011**, *23*, 213001.
(2) Joe, Y. I.; Chen, X. M.; Ghaemi, P.; Finkelstein, K. D.; de la Pena, G. A.; Gan, Y.; Lee, J. C. T.; Yuan, S.; Geck, J.; MacDougall, G. J.; Chiang, T. C.; Cooper, S. L.; Fradkin, E.; Abbamonte, P. Emergence of charge density wave domain walls above the superconducting dome in 1T-$TiSe_2$. *Nat. Phys.* **2014**, *10*, 421−425.
(3) Vaskivskyi, I.; Gospodaric, J.; Brazovskii, S.; Svetin, D.; Sutar, P.; Goreshnik, E.; Mihailovic, I. A.; Mertelj, T.; Mihailovic, D. Controlling the metal-to-insulator relaxation of the metastable hidden quantum state in 1T-TaS_2. *Sci. Adv.* **2015**, *1*, e1500168.
(4) Cai, Y.; Wei, Q.; Huang, F.; Lin, S.; Chen, F.; Gao, W. Thermal stability, latent heat and flame retardant properties of the thermal energy storage phase change materials based on paraffin/high density polyethylene composites. *Renewable Energy* **2009**, *34*, 2117−2123.
(5) Xi, X.; Zhao, L.; Wang, Z.; Berger, H.; Forró, L.; Shan, J.; Mak, K. F. Strongly enhanced charge-density-wave order in monolayer $NbSe_2$. *Nat. Nanotechnol.* **2015**, *10*, 765−769.
(6) Calandra, M.; Mazin, I. I.; Mauri, F. Effect of dimensionality on the charge-density wave in few-layer $NbSe_2$. *Phys. Rev. B: Condens. Matter Mater. Phys.* **2009**, *80*, 241108.
(7) Li, L. J.; O'Farrell, E. C. T.; Loh, K. P.; Eda, G.; Özyilmaz, B.; Castro Neto, A. H. Controlling many-body states by the electric-field effect in a two-dimensional material. *Nature* **2015**, *529*, 185−189.
(8) Yu, Y.; Yang, F.; Lu, X. F.; Yan, Y. J.; Cho, Y.-H.; Ma, L.; Niu, X.; Kim, S.; Son, Y.-W.; Feng, D.; Li, S.; Cheong, S.-W.; Chen, X. H.; Zhang, Y. Gate-tunable phase transitions in thin flakes of 1T-TaS_2. *Nat. Nanotechnol.* **2015**, *10*, 270−276.
(9) Chen, P.; Chan, Y. H.; Fang, X. Y.; Zhang, Y.; Chou, M. Y.; Mo, S. K.; Hussain, Z.; Fedorov, A. V.; Chiang, T. C. Charge density wave transition in single-layer titanium diselenide. *Nat. Commun.* **2015**, *6*, 8943.
(10) Aboutalebi, S. H.; Gudarzi, M. M.; Zheng, Q. B.; Kim, J.-K. Spontaneous formation of liquid crystals in ultralarge graphene oxide dispersions. *Adv. Funct. Mater.* **2011**, *21*, 2978−2988.
(11) Zhi, C.; Bando, Y.; Tang, C.; Kuwahara, H.; Golberg, D. Large-scale fabrication of boron nitride nanosheets and their utilization in polymeric composites with improved thermal and mechanical properties. *Adv. Mater.* **2009**, *21*, 2889−2893.
(12) Cong, C.; Shang, J.; Wu, X.; Cao, B.; Peimyoo, N.; Qiu, C.; Sun, L.; Yu, T. Synthesis and optical properties of large-area single-crystalline 2D semiconductor WS_2 monolayer from chemical vapor deposition. *Adv. Opt. Mater.* **2014**, *2*, 131−136.
(13) Choy, K. L. Chemical vapour deposition of coatings. *Prog. Mater. Sci.* **2003**, *48*, 57−170.
(14) Hou, X.; Choy, K. L. Processing and applications of aerosol-assisted chemical vapor deposition. *Chem. Vap. Deposition* **2006**, *12*, 583−596.
(15) Gong, Y.; Lin, J.; Wang, X.; Shi, G.; Lei, S.; Lin, Z.; Zou, X.; Ye, G.; Vajtai, R.; Yakobson, B. I.; Terrones, H.; Terrones, M.; Tay; Beng, K.; Lou, J.; Pantelides, S. T.; Liu, Z.; Zhou, W.; Ajayan, P. M. Vertical and in-plane heterostructures from WS_2/MoS_2 monolayers. *Nat. Mater.* **2014**, *13*, 1135−1142.
(16) Najmaei, S.; Liu, Z.; Zhou, W.; Zou, X.; Shi, G.; Lei, S.; Yakobson, B. I.; Idrobo, J.-C.; Ajayan, P. M.; Lou, J. Vapour phase growth and grain boundary structure of molybdenum disulphide atomic layers. *Nat. Mater.* **2013**, *12*, 754−759.
(17) Lee, Y. H.; Zhang, X. Q.; Zhang, W.; Chang, M. T.; Lin, C. T.; Chang, K. D.; Yu, Y. C.; Wang, J. T. W.; Chang, C. S.; Li, L. J.; Lin, T. W. Synthesis of large-area MoS_2 atomic layers with chemical vapor deposition. *Adv. Mater.* **2012**, *24*, 2320−2325.
(18) Zhang, Y.; Zhang, Y.; Ji, Q.; Ju, J.; Yuan, H.; Shi, J.; Gao, T.; Ma, D.; Liu, M.; Chen, Y.; Song, X.; Hwang, H. Y.; Cui, Y.; Liu, Z. Controlled growth of high-quality monolayer WS_2 layers on sapphire and imaging its grain boundary. *ACS Nano* **2013**, *7*, 8963−8971.
(19) Liu, Z.; Ma, L.; Shi, G.; Zhou, W.; Gong, Y.; Lei, S.; Yang, X.; Zhang, J.; Yu, J.; Hackenberg, K. P.; Babakhani, A.; Idrobo, J. C.; Vajtai, R.; Lou, J.; Ajayan, P. M. In-plane heterostructures of graphene and hexagonal boron nitride with controlled domain sizes. *Nat. Nanotechnol.* **2013**, *8*, 119−124.
(20) Liu, Z.; Gong, Y.; Zhou, W.; Ma, L.; Yu, J.; Idrobo, J. C.; Jung, J.; MacDonald, A. H.; Vajtai, R.; Lou, J.; Ajayan, P. M. Ultrathin high-temperature oxidation-resistant coatings of hexagonal boron nitride. *Nat. Commun.* **2013**, *4*, 2541.
(21) Sipos, B.; Kusmartseva, A. F.; Akrap, A.; Berger, H.; Forro, L.; Tutis, E. From Mott state to superconductivity in 1T-TaS_2. *Nat. Mater.* **2008**, *7*, 960−965.
(22) Tsen, A. W.; Hovden, R.; Wang, D.; Kim, Y. D.; Okamoto, J.; Spoth, K. A.; Liu, Y.; Lu, W.; Sun, Y.; Hone, J. C.; Kourkoutis, L. F.; Kim, P.; Pasupathy, A. N. Structure and control of charge density waves in two-dimensional 1T-TaS_2. *Proc. Natl. Acad. Sci. U. S. A.* **2015**, *112*, 15054−15059.
(23) Yoshida, M.; Zhang, Y.; Ye, J.; Suzuki, R.; Imai, Y.; Kimura, S.; Fujiwara, A.; Iwasa, Y. Controlling charge-density-wave states in nano-thick crystals of 1T-TaS_2. *Sci. Rep.* **2014**, *4*, 7302.
(24) Cho, D.; Cheon, S.; Kim, K.-S.; Lee, S. H.; Cho, Y. H.; Cheong, S. W.; Yeom, H. W. Nanoscale manipulation of the Mott insulating state coupled to charge order in 1T-TaS_2. *Nat. Commun.* **2016**, *7*, 10453.
(25) Pillo, T.; Hayoz, J.; Berger, H.; Grioni, M.; Schlapbach, L.; Aebi, P. Remnant fermi surface in the presence of an underlying instability in layered 1T TaS_2. *Phys. Rev. Lett.* **1999**, *83*, 3494−3497.
(26) Wu, X. C.; Tao, Y. R.; Gao, Q. X. Fabrication of TaS_2 nanobelt arrays and their enhanced field-emission. *Chem. Commun.* **2009**, 6008−6010.
(27) Li, L. J.; Lu, W. J.; Liu, Y.; Qu, Z.; Ling, L. S.; Sun, Y. P. Influence of defects on charge−density−wave and superconductivity in 1T-TaS_2 and 2H-TaS_2 systems. *Phys. C* **2013**, *492*, 64−67.
(28) Peters, E. S.; Carmalt, C. J.; Parkin, I. P.; Tocher, D. A. Aerosol-assisted chemical vapor deposition of NbS_2 and TaS_2 thin films from pentakis(dimethylamido)metal complexes and 2-methylpropanethiol. *Eur. J. Inorg. Chem.* **2005**, *2005*, 4179−4185.
(29) Zeng, Z.; Tan, C.; Huang, X.; Bao, S.; Zhang, H. Growth of noble metal nanoparticles on single-layer TiS_2 and TaS_2 nanosheets for hydrogen evolution reaction. *Energy Environ. Sci.* **2014**, *7*, 797−803.
(30) Perfetti, L.; Loukakos, P. A.; Lisowski, M.; Bovensiepen, U.; Berger, H.; Biermann, S.; Cornaglia, P. S.; Georges, A.; Wolf, M. Time evolution of the electronic structure of 1T TaS_2 through the insulator-metal transition. *Phys. Rev. Lett.* **2006**, *97*, 067402.
(31) Tersoff, J. Anomalous corrugations in scanning tunneling microscopy: Imaging of individual states. *Phys. Rev. Lett.* **1986**, *57*, 440−443.
(32) Duffey, J. R.; Kirby, R. D.; Coleman, R. V. Raman scattering from 1T-TaS2. *Solid State Commun.* **1976**, *20*, 617−621.
(33) Sugai, S.; Murase, K.; Uchida, S.; Tanaka, S. Comparison of the soft modes in tantalum dichalcogenides. *Physica B+C* **1981**, *105*, 405−409.
(34) Uchida, S.; Sugai, S. Infrared and Raman studies on commensurate CDW states in transition metal dichalcogenides. *Physica B+C* **1981**, *105*, 393−399.
(35) Gasparov, L. V.; Brown, K. G.; Wint, A. C.; Tanner, D. B.; Berger, H.; Margaritondo, G.; Gaál, R.; Forró, L. Phonon anomaly at the charge ordering transition in 1T-TaS_2. *Phys. Rev. B: Condens. Matter Mater. Phys.* **2002**, *66*, 094301.
(36) Yoshida, M.; Suzuki, R.; Zhang, Y.; Nakano, M.; Iwasa, Y. Memristive phase switching in two-dimensional 1T-TaS_2 crystals. *Sci. Adv.* **2015**, *1*, e1500606.

DOI: 10.1021/acs.chemmater.6b02334
Chem. Mater. XXXX, XXX, XXX−XXX